Uranium(VI) Complexes of Glutathione Disulfide Forming in Aqueous Solution

Kretzschmar, J.; Strobel, A.; Haubitz, T.; Drobot, B.; Steudtner, R.; Barkleit, A.; Brendler, V.; Stumpf, T.;

Originally published:

April 2020

Inorganic Chemistry 59(2020)7, 4244-4254

DOI: https://doi.org/10.1021/acs.inorgchem.9b02921

Uranium(VI) complexes of glutathione disulfide forming in aqueous solution

Jerome Kretzschmar,* Alexander Strobel,† Toni Haubitz,‡ Björn Drobot, Robin Steudtner, Astrid Barkleit, Vinzenz Brendler, Thorsten Stumpf

Helmholtz-Zentrum Dresden-Rossendorf, Institute of Resource Ecology, Bautzner Landstr. 400, 01328 Dresden, Germany

Supporting Information Placeholder

ABSTRACT: The interaction between glutathione disulfide, GSSG, the redox partner and dimer of the intracellular detoxification agent glutathione, GSH, and hexavalent uranium, U(VI), were extensively studied by solution NMR (in D_2O), complemented by time-resolved laser-induced fluorescence (TRLFS) and IR spectroscopies. As expected for the hard Lewis acid U(VI), coordination facilitates by the ligands' O-donor carboxyl groups. However, owing to the adjacent cationic α-amino group, the glutamyl-COO reveal monodentate binding, while the COO of the glycyl residues show bidentate coordination. The log *K* value for the reaction $UO_2^{2+} + H_3GSSG^- \rightarrow UO_2(H_3GSSG)^+$ (pH 3, 0.1 M $NaClO_4$) was determined for the first time, being 4.81 ± 0.08; extrapolation to infinite dilution gave log K^e = 5.24 ± 0.08. U(VI) and GSSG form precipitates in the whole pD range studied (2 – 8), showing least solubility for 4 < pD < 6.5. Thus, particularly GSSG – hereby representing also other peptides and small proteins – affects the mobility of U(VI), strongly depending on speciation of either component.

INTRODUCTION

The tripeptide glutathione, GSH, consists of the amino acids L-glutamic acid (Glu), L-cysteine (Cys), and glycine (Gly). A remarkable feature of GSH is its isopeptide linkage between the Glu side chain carboxyl group and the Cys α-amino group, rendering the peptide's N-terminus to possess an adjacent α-carboxyl group (Figure 1, top). GSH is a ubiquitous antioxidant found in human, animal, and plant cells as well as in archaea and bacteria.[1-3] In mammalian cells concentrations as high as 12 mM are reported.[4] Together with its oxidized counterpart and dimer glutathione disulfide, GSSG (Figure 1, bottom), both molecules are paramount for intracellular redox state maintenance.

Radionuclide influxes into the environment are diverse. Naturally occurring radioactive material (NORM) like Th, U, and Ra can dissolve into ground water merely by weathering of soils and rocks. Technologically enhanced NORM originating from ore mining and processing, geothermal engineering, oil and gas production, drinking and wastewater treatment, as well as fertilizer production, can also migrate into the biogeosphere. Moreover, U is still an important source for electrical power supply as the main constituent of nuclear fuel[5, 6] and, therefore, key element of the U processing cycle.[7] Finally, environmental problems also arise from nuclear incidents and the military use of ammunition containing depleted uranium.[8, 9] Comprehensive examination of radionuclide interaction with the environment is mandatory as they can enter the food chain and cause detrimental effects.

Irrespective of naturally occurring conditions, understanding the chemical and physical basics driving radionuclide behavior by studying straightforward model systems in controlled setting, and upon variation of selected parameters, the influence of the various effects can be assessed individually. This approach is essential to understand the processes on a molecular level and to predict a system's behavior for changing conditions.

Under aqueous aerobic conditions uranium typically occurs in hexavalent state, U(VI), in general forming water soluble and, thus, mobile species. As a prominent and characteristic feature in +V and +VI oxidation states, in aqueous phase uranium (and other actinides) form linear dioxo cations ($D_{\infty h}$), that is actinyl ions (AnO_2^{n+}), with ligand coordination limited to the equatorial plane. In contrast, under reducing conditions U is present in its tetravalent state, forming spherical U^{4+} ions.

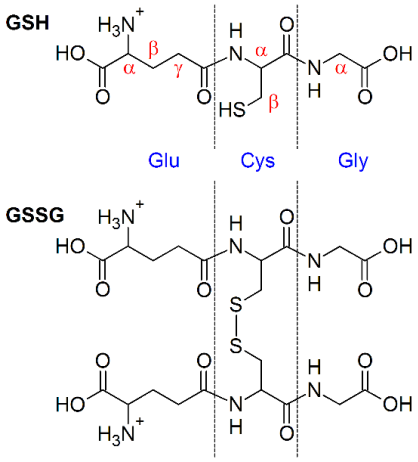

Figure 1. Generic structures of glutathione (GSH) and glutathione disulfide (GSSG) depicted as completely protonated species, with constituting amino acids L-glutamic acid (Glu), L-cysteine (Cys), and glycine (Gly), and positions therein as indicated.

Because of its diverse functional groups, GSH can act as both reductant and complexation agent, being involved in numerous processes for the conjugation of xenobiotics and the detoxification of reactive oxygen species and heavy metal ions.[10-13] U(VI) uptake into cells causes a reduction of U(VI) to U(IV),[14] accompanied by increased GSSG levels, also known as oxidative stress,[15-17] Although GSSG bears no reduced SH group, it is still capable of heavy metal complexation owing to its COO and NH_2 functionalities. *In vivo*, actinides are bound to and transported with a protein fraction, viz. metal-transferrin complexes, as well as a fraction of low-mass molecules like amino acids and carboxylates.[18-20] GSH and GSSG

are both widespread and abundant biomolecules of high importance as being critical parts in cell regulation and detoxification mechanisms. Studying their interaction with actinides is of great interest, extending into spectroscopic characterizations as model molecules. Most papers investigating GSH and GSSG metal ion interaction, i.e., structures and thermodynamic constants, focused on transition metal ions,[21-28] whereas only few studies address U(VI) interaction.[14, 29-32] Thus, for U(VI) in aqueous solution in general, and by complementary spectroscopies in particular, the present study allows critical insights into complex structures and speciation. The herein presented results concentrate on GSSG as the ligand, for discussion and comparison GSH related results are included, or provided as Supporting Information (SI). These studies also complement the recently published formation of hyperstoichiometric UO_{2+x} phases after a redox reaction in the GSH/GSSG–U(VI) system.[33]

For species distribution diagrams for the applied components, refer to Figures S1 and S2, SI. Table 1 shows literature pK_a values for both ligands. Note that GSSG reveals the double amount of carboxyl and amino functionalities (I and II) since being the dimerized species.

Furthermore, GSSG's two GS moieties are spectroscopically equivalent because of a C_2 axis through its S–S bond, as also observed in the X-ray structre,[34] upon which both moieties generate an identical set of ^{1}H NMR signals. Since GSH and GSSG comprise chiral Glu and Cys, and prochiral Gly, all methylene groups are diastereotopic. Thus, the latter possess chemically distinct hydrogen atoms, consequently causing different ^{1}H NMR signals.

Table 1. Logarithmic deprotonation constants of GSH[35] and GSSG[36] (25 °C, 0.15 M KCl).

ligand		pK_a			
		COOH		SH	NH_3^+
		Glu	Gly		
GSH		2.22 ± 0.01	3.52 ± 0.01	8.78 ± 0.01	9.65 ± 0.01
GSSG	(I)	1.6 ± 0.1	3.15 ± 0.02	–	8.83 ± 0.01
	(II)	2.23 ± 0.03	3.85 ± 0.01	–	9.53 ± 0.02

EXPERIMENTAL SECTION

Materials

Caution: Uranium is a radioactive material! All preparation steps were performed with safety precautions according to both radio- and chemotoxicity of natural uranium (U-nat.). 200 mM stock solutions of U(VI) were prepared by dissolution of 1.3096 g $UO_3 \cdot 2.3H_2O$ (U-nat, A = 25.5 kBq g^{-1}) in 20 mL 0.5 M DCl. Sample series (variations of pD and metal-to-ligand ratio, M/L) were obtained by mixture of proper aliquots of the U(VI) stock solution and freshly prepared stock solutions of either GSH or GSSG under continuous stirring with pD control (Xylem Analytics WTW inoLab® pH Level 1 and pH 540 GLP pH-meters with Schott Instruments Blue Line 16 pH electrodes), and adjustment towards final pD (2–8 for GSSG, 2–10 for GSH), with pD = pH + 0.4.[37, 38] Samples of varying pD were prepared with 10 and 100 mM total GSSG concentration, and M/L of 0.5 and 0.05 for either series. A series of varying M/L in the range 0.05 – 10 was prepared at constant pD = 2. GSH samples were prepared with 6.7 mM ligand concentration and M/L of 0.5 and 2 for pD-dependent series, as well as varying [U(VI)] for constant pD values of 2, 5, and 8. Since GSH–U(VI) samples are subject to redox reaction studies, GSH containing samples were handled under N_2 atmosphere in a glovebox, and transferred to 5 mm screw-cap NMR tubes (Deutero). Since both components are already present in their oxidized form, GSSG–U(VI) samples were prepared and handled under ambient conditions.

Because of precipitation, after pD adjustment and equilibration under continued stirring, the suspensions were centrifuged for 15 min at 14400 × g (Beckman Coulter Avanti j-20 XP centrifuge, for GSH samples) or for 1 h at 5500 × g (Sigma 3K18 centrifuge, GSSG samples). Resulting supernatants were carefully removed by a pipette and, where necessary, pD values were adjusted prior to solution NMR spectroscopy.

The supernatants were analyzed regarding their [U(VI)] by means of ICP-MS (Elan 9000, Perkin Elmer). Selected corresponding precipitates were re-dispersed, washed three times with 1 M NaCl solution and repeatedly centrifuged, discarding the thereby accruing supernatants, and after lyophilization further analyzed by FT-IR spectroscopy. Fractions of both supernatants and precipitates obtained from the GSSG–U(VI) NMR sample preparation were used for time-resolved laser-induced fluorescence spectroscopy (TRLFS). The precipitates collected after (initial) centrifugation were re-dispersed by ultrasonication, then iteratively washed twice with 1 M $NaClO_4$ solution and centrifuged (with supernatants discarded). Both the washed bright yellow precipitates dispersed in 1 M $NaClO_4$ and the decanted supernatants were transferred to plastic cuvettes, deep-frozen by liquid N_2, and subsequently investigated by TRLFS, showing consistent results regardless of preparation procedure.

Samples intended for stability constant determination by TRLFS (at 25 °C) were prepared using Milli-Q water. Aliquots of a 98 mM $UO_2(ClO_4)_2$ stock solution were further diluted and admixed to appropriate amounts of a 0.8 mM GSSG stock solution under continuous stirring, with 0.1 M $NaClO_4$ (p.a., Merck) for total ionic strength maintenance. The ligand titration series at constant pH = 3 contained 500 μM U(VI) and 0, 5, 10, 40, 70, 100, 150, or 200 μM GSSG. pH was adjusted by NaOH and $HClO_4$ utilizing the above stated equipment. pH measurement with potentially chloride (a luminescence quencher) leaking electrodes was performed with a second set of samples obtained by halving the initial samples' volume to obtain two subsets of identical volume and composition. The required amounts of NaOH and $HClO_4$, respectively, were then applied to adjust the pH in the TRLFS samples.

Methods

NMR spectroscopy. GSSG spectra were obtained on a Varian Unity Inova 400 (9.4 T) spectrometer with resonance frequencies of 400.1 and 100.6 MHz for ^{1}H and ^{13}C, respectively, using a 5 mm direct detection broadband probe. Spectra of GSH were acquired on an Agilent DD2 600 spectrometer (14.1 T; 599.8 and 150.8 MHz ^{1}H and ^{13}C resonance frequencies, respectively), using a 5 mm oneNMR™ probe. Occasionally the water signal was suppressed by a 2 s pre-saturation pulse with offset on the water resonance, the latter depending on sample composition and pD; ^{13}C spectra were acquired with ^{1}H broadband decoupling, ^{13}C{^{1}H}. ^{1}H and ^{13}C chemical shifts are reported relative to the methyl signal (δ_H, δ_C 0.0 ppm) of DSS (sodium 2,2-dimethyl-2-silapentane-5-sulfonate, Aldrich, 97%)

Luminescence spectroscopy. U(VI) luminescence was induced by a Nd:YAG laser system (Minilite, Continuum) using pulses at 266 nm excitation wavelength, 10 Hz repetition rate, and of 500 μJ averaged energy. The emitted luminescence light was collected perpendicular to the direction of excitation, focused into a spectrograph and an ICCD camera system (both Horiba Jobin Yvon) in the range 400–650 nm with a resolution of 0.3 nm. Time-resolved spectra were recorded by acquisition of 100 spectra at delay times between 0 and 1500 μs, with increments of 50 μs, and the initial delay set to 0.1 μs. A cryostat (Oerlikon Leybold) was used for temperature stability at 153 K (−120 °C). The deep-frozen U(VI)–

GSSG supernatants and precipitates were removed from their plastic cuvettes and then, as an ice cube, transferred to an in-house built sample holder (metal block with a sample insertion hole and three windows for laser irradiation and luminescence emission detection).

Factor Analysis. Parallel factor analysis [39, 40] was used for TRLFS data deconvolution. Accordingly, the N-way toolbox for matlab[41] was used as previously described for other TRLFS data.[42-44]

FT-IR spectroscopy. Obtained U(VI) precipitates were prepared as KBr discs for IR spectra acquisition with a Perkin Elmer Spektrum 2000 spectrometer in the range between 6000 and 500 cm^{-1}.

RESULTS

Upon exceeding pD 3 during sample preparation, a solid phase precipitated. After centrifugation, both the aqueous and the solid phase were treated and considered separately in the following. Note that, for internal consistency, the FT-IR and TRLF spectra are denoted by that pD for which both precipitate (although washed with ^1H_2O) and supernatant were obtained.

Solution studies

NMR spectroscopy with GSSG. All NMR spectra in this work are characterized by mole fraction weighted average signals, indicating a ligand exchange fast on the NMR time scale. The complexes are hence considered kinetically labile. Therefore, upon successive addition of metal ion or increasing pD, the free ligand concentration decreases and that of the ligand bound to U(VI) increases. Correspondingly, the observed signals shift toward those chemical shift values respectively associated with the complex.

At pD 2 the interaction between U(VI) and GSSG is primarily determined by the Glu carboxyl group as revealed by both ^1H and $^{13}C\{^1H\}$ NMR spectra in Figures 2 and 3, respectively. Upon increasing [U(VI)], the ^1H signals associated with the Glu residue show the largest U(VI) complexation-induced chemical shift changes, $\Delta_U\delta = \delta_{sample} - \delta_{blank}$. The Gly α ^1H signal exhibits some significant shift (and broadening) only for the highest [U(VI)]. In contrast, signals due to the Cys residue are shifted upfield, hence showing negative $\Delta_U\delta_H$, and are in principle the least affected. Corresponding numerical values are given in Table S1, SI. For pD 2 nearly all initial U(VI) and GSSG remain dissolved. However, already at pD ≥ 3 only parts of both dissolved GSSG and U(VI) are present in solution. Notably, for a series initially 10 mM in GSSG and 100 mM in U(VI), at pD 4 and 5 no ligand signals are detectable, cf. Figure S3, SI. The precipitate obtained during sample preparation therefore contains U(VI)-bound GSSG.

Figure 3 depicts the carboxyl region of GSSG, with the blanks' spectra shown in black and those of the initially L/M = 2 sample solutions given in red. For better visibility, related signals are respectively colored. H,C-HMBC spectra (not shown) ensured correct carboxyl and carbonyl ^{13}C signal assignment. Note that the blank's signals themselves shift because of GSSG's pD-dependent speciation and, to a lesser extent, conformation. Thus, it is important to compare spectra of U(VI) containing sample and blank for the same given pD value to appraise the U(VI)-induced effects. Already at pD = 2 UO_2^{2+}interacts strongly with Glu COO as inferred from 0.93 ppm $\Delta_U\delta_C$ (see solid arrow), while Gly COO's $\Delta_U\delta_C$ is only 0.27 ppm. At pD 3 and 4, however, the respective values amount to 0.20 and 0.13 ppm for Glu COO, and 0.76 ppm for Gly COO (either pD, dashed arrows). As of pD 5, for both carboxyl carbons the observed $\Delta_U\delta_C$ decrease to values of 151 through 77 ppb for Gly COO, and 85 ppb for Glu COO, with the signals of the latter exhibiting broadening over the whole pD range. Additionally, the carbonyl carbons associated with the peptide bonds, Glu CO and Cys CO, show slight shifts downfield in the presence of U(VI) relative to the corresponding blanks. An analogous set of spectra recorded for the L/M = 20 sample series as well as the corresponding spectra of the aliphatic carbons are given in Figures S4 and S5, SI, showing similar but smaller site-dependent effects.

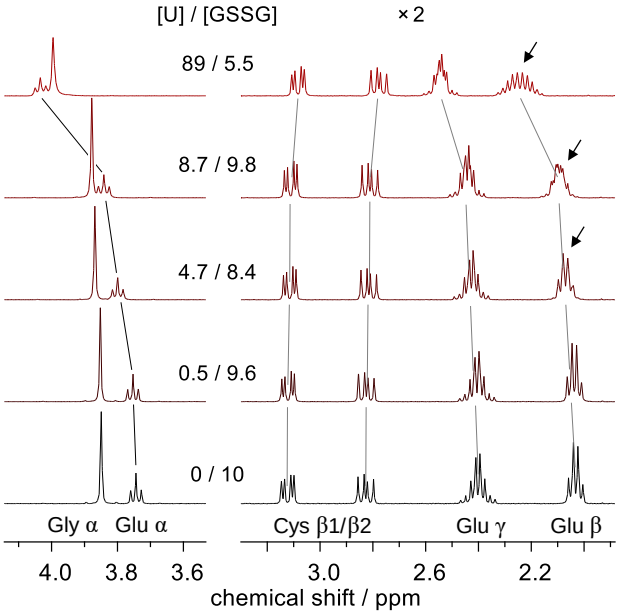

Figure 2. ^1H NMR spectra for pD 2 solutions initially 10 mM in GSSG and at different [U(VI)]. Spectra are labelled with the actual concentrations (in mM). Only regions of interest are depicted, with lines drawn for better visibility. The signals on the right are vertically magnified by a factor of 2.

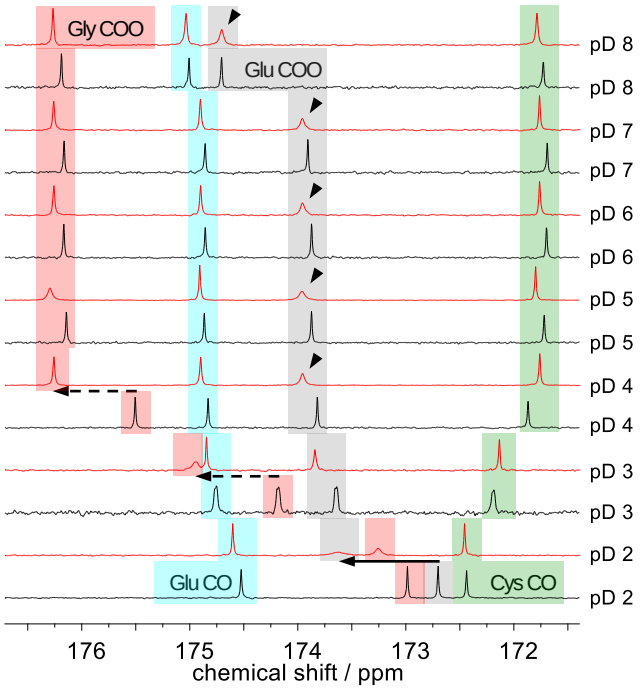

Figure 3. GSSG carboxyl region of pD-dependent $^{13}C\{^1H\}$ NMR spectra of the blanks shown in black and of U(VI) solutions given in red, with initial concentrations of 150 mM GSSG and 75 mM U(VI). Signals are color coded for clarity.

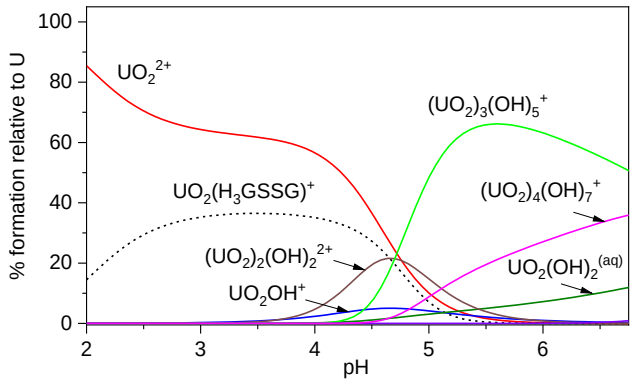

Figure 4. Species distribution of 500 μM U(VI) and 200 μM GSSG in 0.1 M $NaClO_4$ solution (25 °C, N_2 atmosphere), calculated with HySS2009,[45] using the log *K* values of $UO_2(H_3GSSG)^+$ (this work, dashed line), GSSG,[36] and the most updated U(VI) thermodynamic data from NEA TDB.[46]

Luminescence spectroscopy with GSSG. The U(VI) luminescence intensity (500 µM U(VI), pH 3, 25 °C) decreases with increasing GSSG concentration while the position of the emission band are the same for the entire concentration series. This static quenching is caused by the formation of a non-luminescent complex with a simultaneous decrease in the concentration of luminescent free metal ions. Such data could be interpreted using the Stern-Volmer relation, $I_0/I = 1 + K_{SV}$ [Q]. Here I_0 is the intensity without quencher, K_{SV} the Stern-Volmer constant, and [Q] the quencher concentration. The slope K_{SV} of the line (I_0/I –1) vs. [GSSG] defines the association constant *K* of the quenched complex based on the mass action law.[30, 47] We determined the log *K* for the $UO_2(H_3GSSG)^+$ complex as 4.81 ± 0.08. This corresponds to a $\log \beta_{131}$ = 27.02 ± 0.12 (25 °C, 0.1 M $NaClO_4$) for the reaction $UO_2^{2+} + H_3GSSG^- \rightarrow UO_2(H_3GSSG)^+$ (see Figure S6, SI). These values were then extrapolated to infinite dilution, applying the Davies equation,[48] accordingly yielding $\log K^{\circ}$ = 5.24 ± 0.08 and $\log \beta^{\circ}_{131}$ = 29.38 ± 0.12. A correspondingly calculated speciation diagram is shown in Figure 4.

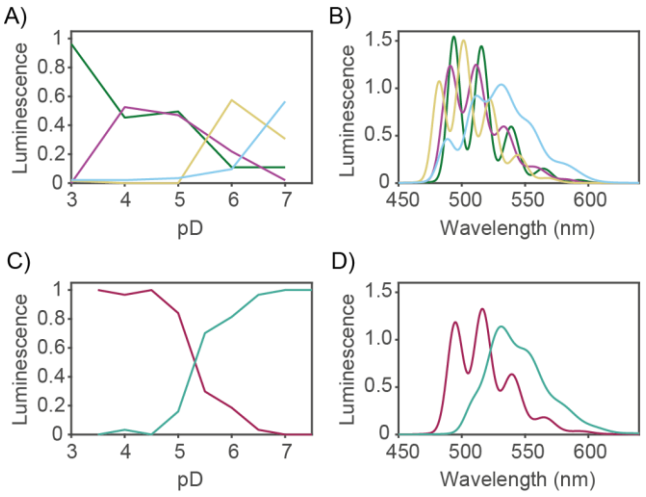

Figure 5. Scaled luminescence-based speciation of U(VI) in the GSSG system from pD 3 through 7 as determined by cryo-TRLFS (left panel), and PARAFAC-extracted emission spectra (right panel) as obtained from the supernatants (A and B) and the precipitates (C and D). Color coding is associated with the species described in Table 2.

Table 2. Luminescence spectroscopic data obtained from cryo-TRLFS of the supernatants and precipitates, together with species assignment related to the graphs depicted in Figure 5. Main peaks are given in bold.

Species	Peak positions (nm)	Luminescence lifetime (μs)
Supernatant		
UO_2OH^+ (aq) (—)	**494**-515-539-565-592	125 ± 5
U(VI)–carbonate (aq) (—)	482-**501**-522-544-568	810 ± 30
U(VI)–GSSG (aq) (—)	491-**511**-534-558-584	160 ± 20
U(VI)–GSSG–OH (aq) (—)	489-510-**531**-555-579	200 ± 15
Precipitate		
U(VI)–GSSG (s) (—)	495-**516**-540-565-594	120 ± 15
U(VI)–GSSG–OH (s) (—)	508-**530**-553-578-606	70 ± 10

The soluble fraction of the U(VI)–GSSG system was then characterized by cryo-TRLFS. It is well known that several quenched U(VI)-complexes become luminescent upon deep freezing. Indeed, four different U(VI)-species could be identified at 153 K. Data deconvolution results (PARAFAC) are shown in Figure 5A and 5B, and Table 2. Four U(VI) species were extracted from the supernatant TRLFS data (top). Based on their emission spectra and luminescence lifetimes (Figures S7–S8, SI, and Table 2) the species were assigned to the 1:1 hydroxo species,[43] UO_2OH^+ (green), a U(VI)–carbonate species[49] (yellow), and two U(VI)–GSSG complexes. The U(VI)–GSSG complex predominating in the acidic pD range corresponds to the binary complex quenched at room temperature (magenta), while as of pD ≈ 5 a further, ternary U(VI)–GSSG–OH complex forms (light blue). The spectral shape and red-shifted main transition of the latter is indicative for a polynuclear species.[50-52] These findings are in excellent agreement with the NMR results, corroborating the nature of this complex being a ternary U(VI) hydroxo GSSG complex.

NMR spectroscopy with GSH. Owing to both structural and chemical similarity to GSSG, in the presence of U(VI) GSH's NMR signals in principle exhibit comparable qualitative effects, e.g., induced signal shifts and line broadenings. The respective spectra and corresponding graphical evaluation, together with further remarks, are provided as Supporting Information (Figures S9–S17, SI). That is, for the lowest pD values the Glu residue related signals are shifted the strongest, whereas for pD ≥ 3 the Gly α ^{1}H signal reveals the largest $\Delta_U\delta_H$, and the magnitude of the Cys $\Delta_U\delta_H$ are smallest overall. Corresponding $\Delta_U\delta_H$ vs. pD plots reveal similar features for either of the M/L = 2 and M/L = 0.5 series, with spectra of the former showing a stronger response. For both series, $|\Delta_U\delta_H|$ values increase upon increasing pD up to ≈ 3.5. However, the curves evince a notable decline in the $|\Delta_U\delta_H|$ values (Figure S17, SI, dashed lines), observed above pD 3.5 and 3.25 for M/L = 0.5 and 2, respectively. Spectra obtained for pD ≥ 6 show only minor U(VI)-induced effects. For the U(VI)–GSH samples showed remarkable precipitation, acquisition of GSH ^{13}C NMR spectra was waived.

Precipitate studies

Luminescence spectroscopy with GSSG. The conclusive GSSG solution analysis is further expanded by investigations of the U(VI)–GSSG precipitates, with the PARAFAC deconvolution results shown in Figure 5 C and D (*vide supra*), and the associated luminescence decays and spectral analyses given in Table 2 and Figure S8, SI. In contrast to the supernatant, the precipitate is adequately described with only two species. The first species (brown) resembles the supernatant's binary U(VI)–GSSG (aq) complex in spectral shape and luminescence lifetime, which can be explained by a comparable U(VI) environment. The spectral shift of 4 nm is attributed to the formation of an amorphous solid phase. As of pD 5, the second species present (cyan) again features a red-shifted spectrum of distinctive appearance, hence ascribed to a polynuclear U(VI)–GSSG–OH (s) ternary complex (cf. Figure 5 B and D, and Table 2). Observation of polynuclear GSSG complex species for both the supernatant and the precipitate correlates with the emergence of polynuclear hydrolysis species in this pD range. These hydrolysis species act most likely as the precursor for the U(VI)–GSSG–OH ternary complex.

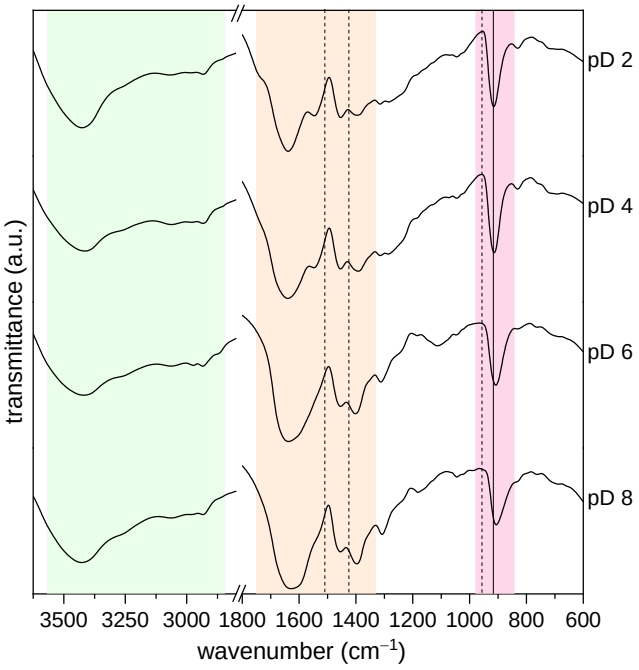

Figure 6. FT-IR spectra (KBr disc) of the precipitates obtained from suspensions initially 150 mM in GSSG and 7.5 mM in U(VI) for pD 2 through 8, highlighting characteristic spectral regions: stretching vibrations of OH, NH, and CH/CH$_2$ (green), C=O (orange), and UO$_2$ (pink); dashed lines indicate band positions for pure-inorganic U(VI) phases (see text).

FT-IR spectroscopy with GSSG. The IR spectra (Figure 6) can be subdivided into three regions of interest: stretching vibrations of OH, NH, and CH/CH$_2$ (green), C=O (orange), and UO$_2$ (pink). By means of the second derivatives a better spectral resolution could be achieved. Evaluation of the FT-IR spectra obtained from the bright yellow precipitates clearly reveals features associated with both GSSG and U(VI). Basically, all spectra are very similar among one another, showing only gradual changes upon increasing pD. For a detailed band assignment, refer to Table S3, SI. Particularly for pD 2 (and pD 4) the (weak) shoulder at 1736 cm^{-1} indicates that GSSG's Gly carboxyl groups are still (partially) protonated. For the whole pD range sampled, the antisymmetric and symmetric stretching carboxylate vibrations, ν_{as} and ν_s, of unbound COO are respectively found at 1592 ± 4 and 1396 ± 1 cm^{-1}. Features associated with U(VI)-bound COO, ν_{as} and ν_s are observed at 1578 ± 3 and 1472 ± 2 cm^{-1} (Gly) and 1637 ± 2 and 1375 ± 3 cm^{-1} (Glu), respectively. Given figures denote mean values and the pD-dependent range of the band position. Moreover, the Glu–Cys and Cys–Gly amide I bands are observed at 1682 ± 1 and 1654 ± 1 cm^{-1}, showing hypsochromic shifts of 20 and 27 cm^{-1}, respectively, relative to the free ligand.[53] The antisymmetric stretching vibration of the uranyl unit, ν_3(UO$_2$), is observed between 916 and 906 cm^{-1} for pD 2–8, respectively (vertical solid line in Figure 6).

DISCUSSION

NMR measurements demonstrated that already at acidic conditions such as pD 2 GSSG (and GSH) interact strongly with UO_2^{2+} as deduced from remarkable $\Delta_U\delta$ (Figures 2 and 3). For both GSSG and GSH, at the lowest pD values the complexation-induced effects are largest for the Glu residue, whereas for pD ≥ 3 the Gly residue associated signals reveal stronger shifts.

This qualitative difference in U(VI) complexation is because of the (cationic) amino group in direct vicinity to the Glu carboxyl, on the one hand causing Coulomb repulsion to the metal ion.[54] On the other hand, electron withdrawal (–I effect) from the COO renders the pK_a to be low (easy accessibility) but the carboxyl group to be less nucleophilic. Complementary, the Gly carboxyl is less acidic, and thus of reduced accessibility due to competition between D^+ and U(VI) for the binding site. Accordingly, at low pD the Gly COO shows the smaller $|\Delta_U\delta|$. However, as of pD values comparable to its pK_a (cf. Table 1), complexation is preferred at this site.

TRLFS measurements showed that the binary GSSG–U(VI) (aq) complex, $UO_2(H_3GSSG)^+$, is non-fluorescing at room-temperature, but can be detected under cryogenic conditions (153 K). Nonetheless, by means of a Stern-Volmer plot its stability constant was determined as $\log K = 4.81 \pm 0.08$, according to $\log \beta_{131} = 27.02 \pm 0.12$, at 25 °C in 0.1 M $NaClO_4$ pH 3 media. The correspondingly calculated species distribution diagram (Figure 4) is excellently in line with the NMR spectral findings from Figure 3, with the strongest complexation-induced chemical shift changes observed for the existence range of $UO_2(H_3GSSG)^+$ complex. The participation of three out of four carboxyl functionalities for complexation mirrors the quite high determined complex stability of $\log \beta^*_{131} = 29.38 \pm 0.12$. Upon comparison with the stability constant of 2.24 ± 0.02 (25 °C, 1 M $NaClO_4$) for the U(VI)–GSH 1:1 complex[29] (corresponding to a $\log \beta_{121}$ of 20.67 ± 0.04), the herein determined stability constant for the U(VI)–GSSG 1:1 complex appears reliable. Based on the higher number of (basic) functional groups in GSSG as compared to GSH, larger values for both the association constant and the overall stability constant for U(VI) complexation by GSSG are plausible.

Upon increasing pD to values above 5, the emission bands associated with GSSG complexation show a basically altered spectral appearance, along with a bathochromic shift and a prolonged lifetime attributed to the formation of polynuclear complexes. Under atmospheric conditions, as of pD > 5 also carbonate species such as $(UO_2)_2CO_3(OH)_3^-$, $UO_2(CO_3)_2^{2-}$, and $UO_2(CO_3)_3^{4-}$ form in aqueous solution, according to $\log \beta^*$ of –0.86, 16.61, and 21.84, respectively (cf. also speciation diagram in Figure S1, SI).[46] According to the remarkably long emission lifetime of 810 ± 30 μs, a U(VI)–carbonate species occurs temporarily (yellow species in Figure 5). The intermediate presence can be explained by the depletion of dissolved ligand at circumneutral conditions owing to precipitation of GSSG complexes. The concentration of metal and ligand remaining in solution (see Figures S18 and S19, SI) is insufficient to compete with dissolved carbonate for U(VI) complexation. However,

upon further increasing pD, and thus increasing contents of dissolved peptide, the U(VI)–carbonate complex is then displaced by polynuclear U(VI)–GSSG–OH species. Regardless of the absolute GSSG concentration, either series with 20-fold ligand excess shows the least amounts of dissolved U(VI) around pD 5 (cf. Figure S18, SI), when GSSG predominates as a dianionic species. The fraction of formed precipitate decreases, i.e., the quantity of soluble U(VI) increases upon further addition of base. This result is ascribed to the formation of anionic polynuclear U(VI)–GSSG–hydroxo species showing an increased solubility.

Interestingly, also ^{13}C NMR spectroscopy can discern the changing GSSG–U(VI) complex speciation. For both Glu and Gly residues the observed $\Delta_U\delta$ values are largest for pD ≤ 4 since UO_2^{2+} causes stronger complexation-induced effects than the eventually emerging U(VI) hydroxo species. Coordination by ligands (Lewis bases) in general or, as in the present case, successive hydrolysis upon raising pD, continuously decreases uranium's Lewis acidity. Accordingly, the (axial) U–O_{yl} bonds increase in length accompanied with a reduced O=U=O bond force constant as reflected by bathochromic shifts of the symmetric ν_1 and antisymmetric ν_3 UO_2 stretching modes in vibrational spectroscopies.[55-58] Therefore, as the electron density around the probed nuclei correlates with the chemical shift, coordination to (polynuclear) U(VI) hydrolysis species causes much less electron withdrawal from GSSG's carboxyl carbons, for instance, resulting in smaller differences between sample and blank spectrum.

For both L/M = 2 and 20 GSSG sample series ^{13}C NMR signals indicate interaction of Glu and Gly carboxyl with U(VI) up to pD 8 with some small induced shifts, taking into account the spectral implications concerning the steadily decreasing Lewis acidity of U(VI). Similar line broadenings observed for analogous signals indicate the same molecular dynamics in both series. Spectra of GSSG–U(VI) solutions reveal broadened Glu COO ^{13}C signals for the whole pD range (2–8), while the signals due to Gly COO are broadened only for pD ≤ 5. (cf. spearheads in Figure 2). As described in more detail for GSH (*vide infra*), line broadening is indicative of a reduced exchange reaction rate at the binding sites. Accordingly, U(VI) resides longer at the Glu carboxylates than at the Gly carboxylates (kinetics). The latter is ascribed to Glu amino groups hydrogen bonding in the second coordination shell, constituting a kind of pseudobridging, i.e., monodentate carboxyl coordination accompanied by a hydrogen bond between the amino group and an aqua or hydroxo ligand of the uranyl unit. Similar binding motifs are already inferred from experiment and calculation in other model systems.[59-61] Moreover, simultaneous (chelating) interaction between (polynuclear) U(VI) species and both Glu residues is conceivable, as inferred from GSSG's conformation resolved from single-crystals (Figure S20, SI). A corresponding motif is respected for the suggested structure of the binary complex given in Figure 7 (below). Investigations by, e.g., Reitz et al.[62] and Barkleit et al.[63] regarding U(VI) interaction with S-layer proteins and peptidoglycan, respectively, also raised the question whether amino groups are involved in coordination. Particularly the diaminopimelic acid in peptidoglycan is structurally very similar to the Glu moieties, as either possesses a $(CH_2)_2CH(NH_3^+)COO^-$ residue.

Considering the speciation of both U(VI) and GSSG, up to pD 4 the complexes are binary; for pD 2 forming between UO_2^{2+} and Glu's COO, and as of pD 3 UO_2^{2+} binds to both Glu's and Gly's carboxyl groups. Thus, $[(UO_2)(OOC)GSSG(COO)_n(COOH)_{3-n}]^{(3-n)+}$ (n = 0, 1, 2, 3) is a general representation of the binary species. In case of n = 3, the resulting net neutral species likely precipitates.

Regarding the precipitates, both FT-IR and TRLFS reveal excellent agreement for the coordination and speciation (changes) observed along the pD-dependent series.

Evaluation of the carbonyl region (~ 1700–1350 cm^{-1}) in the FT-IR spectra is somewhat challenging for the ratio of chemically active carboxyl groups to backbone amide groups is high. Therefore, the simultaneous occurrence of COOU, COO^-, COOH, and CONH further increases the number of bands. Hence, the respective spectral region is characterized by overlapping absorptions resulting in a broad feature. The degree of spectral splitting, $\Delta\nu(\nu_{as}, \nu_s)$, allows to derive the carboxylate groups' type of coordination. The $\Delta\nu$ value of the uncomplexed ligand serves as reference, in the present case 196 cm^{-1}. In general, bidentate coordination shows a lower spectral splitting, whereas monodentate coordination usually exhibits a larger band separation as compared to the uncomplexed ligand.[64] The obtained $\Delta\nu$ of 106 cm^{-1} indicates bidentate (COO)<U(VI) binding. There are, however, particularly for pD 2, two absorptions in the region of interest that cannot be ascribed to vibrational modes of free GSSG, namely at 1637 and 1375 cm^{-1}. Referring these bands to ν_{as} and ν_s (COOU), $\Delta\nu$ is calculated to about 260 cm^{-1}, a value characteristic for monodentate O=CO–U(VI) coordination.[64-66] Carboxyl–U(VI) ligation is reported to be bidentate for carboxylates such as aliphatic acetate,[66] propionate,[67, 68] *n*-valerate,[69] or aromatic benzoate and phthalate,[67, 70] and even for glutamate and aspartate in case of binding by their respective side-chain carboxylate.[71] Other amino acids such as alanine or glycine, however, show monodentate coordination in their zwitterionic form.[72-74] For the ligands' Gly terminus acts like a conventional carboxylic acid and while the Glu terminus constitutes a zwitterion, it is concluded that U(VI)-coordination by the Gly COO is bidentate and by the Glu COO is monodentate. The latter occurs especially for acidic conditions for which the Gly carboxyl group is not yet accessible. Figure 7 depicts a suggested molecular structure for $UO_2(H_3GSSG)^+$, assuming a pentagonal bipyramidal U(VI) coordination geometry and the occupation of the fifth equatorial coordination site by a water ligand.

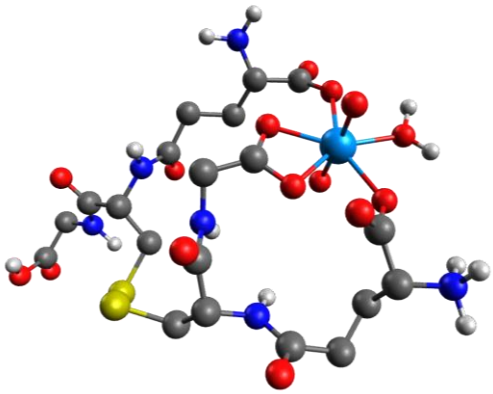

Figure 7. Proposed molecular structure of $UO_2(H_3GSSG)^+$ predominating under acid conditions; light blue, uranium; dark grey, carbon; white, hydrogen; dark blue, nitrogen; red, oxygen; yellow, sulfur; carbon-bound hydrogen atoms are omitted for clarity.

Accordingly, ^{1}H NMR spectroscopy reveals further indications for Glu's monodentate binding upon alteration of the splitting pattern particularly of the Glu β signals (Figure 2, marked by arrows). As the signals are mole fraction weighted averages, upon increasing U(VI) contents the observed spectra increasingly reflect the formed complex. The Glu β CH_2 signals change from GSSG blank-dominated pseudo-quartet appearance to a higher-order multiplet due to the GSSG–U(VI) complex. For these methylene hydrogen atoms are diastereotopic, they are sensitive to changes in local symmetry and chemical environment as is the case particularly for monodentate binding. Consequently, the individual hydrogen atoms become more distinct and so do their corresponding chemical shifts. Also

the signals of the adjacent Glu γ methylene hydrogen atoms are affected due to altered HC(β)–(γ)CH torsion angles, thus also changing the vicinal coupling constants.

Theoretical studies[60] indicated that mono- and bidentate coordination are essentially isoenergetic in solution. After thermodynamic correction, however, bidentate coordination was shown to be clearly favored largely due to entropy effects upon liberation of two water molecules in contrast to only one water ligand as for monodentate carboxylate binding.

For any ligand binding to U(VI) results in a bathochromic shift of the stretching frequencies, stepwise ligand coordination progressively reduces the $\nu_3(UO_2)$ of 961 cm^{-1} for free UO_2^{2+} as shown for, e.g., 1:1, 1:2, and 1:3 U(VI)–acetate complexes with absorptions found at 949, 939, and 924 cm^{-1}, respectively.[66] Since the presence of U(VI) hydroxo species is considered unlikely for the pD 2 sample, and the respective FT-IR spectrum discloses features unambiguously associated with GSSG, it is concluded that the precipitate obtained at pD 2 consists of a binary U(VI)–GSSG (s) complex. Regarding the low $\nu_3(UO_2)$ of 916 cm^{-1} observed at pD 2, the UO_2^{2+} is concluded to be monodentately coordinated by two Glu carboxyl groups as the Gly COOH are protonated more than 93% under these conditions (ν_{as} of COOH at 1736 cm^{-1}), and monodentate binding induces stronger $\nu_3(UO_2)$ red-shifts.[55-58, 60]

Upon increasing pD, the occurrence of hydrolysis species and coincidental accessibility of the Gly carboxylates renders the observed $\nu_3(UO_2)$ to change only little (916 through 906 cm^{-1} for pD 2 through 8, respectively) because of compensating effects (cf. solid black line in Figure 6). On the one hand, the bidentately coordinating Gly carboxylates cause a smaller decrease in $\nu_3(UO_2)$ alike bidentate acetate coordination (see above). On the other hand, and in line with their predominance observed in TRLF spectra, (polynuclear) U(VI) hydrolysis species are themselves characterized by lowered $\nu_3(UO_2)$. Compared to the 961 cm^{-1} for free UO_2^{2+}, U(VI) hydrolysis causes notable $\nu_3(UO_2)$ red-shifts, e.g., 943 and 923 cm^{-1} attributed to $(UO_2)_2(OH)_2^{2+}$ and $(UO_2)_3(OH)_5^{+}$, respectively.[56, 75] Therefore, the observed pD-dependent gradual decrease of $\nu_3(UO_2)$ is due to a decreasing fraction of the net neutral U(VI)–GSSG (s) binary species, and an increasing fraction of (polynuclear) U(VI)–GSSG–hydroxo (s) ternary species. This IR-based conclusion is corroborated by the results obtained from TRLFS in combination with PARAFAC, allowing for a sufficient description of the precipitates by two species only (Figure 5, bottom row). That is, upon increasing pD, contents of the binary GSSG complex (brown) decreases while the fraction of the ternary (polynuclear) GSSG complex (cyan) increases.

Considering the speciation of both U(VI) and GSSG for any given pH value, it is particularly the pH region of about 4 through 6.5, for which the forming net neutral precipitates do not require any counter ions for charge balancing. At low / high pH values, however, complexes formed by the simultaneously occurring U(VI) and GSSG species require, e.g., Cl^- or Na^+, respectively, for the formation of net neutral precipitates. This likely explains the increased solubility of the respectively formed complexes below pD 4 and above 6.5 (cf. Figure S18, SI).

Moreover, the precipitates do not contain carbonate species as evidenced by the strong bathochromic shift of the emission lines and the overall shorter luminescence lifetimes. This conclusion is corroborated by the absence of FT-IR features characteristic for vibrational modes of both metal and ligand in uranyl carbonate species. Solid UO_2CO_3 (rutherfordine) causes an intense and broad $\nu_3(UO_2)$ absorption band ranging from 990 through 866 cm^{-1} centered at 950 cm^{-1}, as well as apparent $\nu_{as}(CO_3)$ and $\nu_s(CO_3)$ at about 1510 and 1420 cm^{-1}, respectively,[76, 77] and metaschoepite ($UO_3 \cdot nH_2O$, $n < 2$) gives rise to a strong $\nu_3(UO_2)$ absorption at 958 cm^{-1}.[78] Although [U(VI)] are applied in the millimolar range, and U(VI) solubility may be exceeded, no such uranyl containing inorganic phases precipitated according to the absence of corresponding band positions (dashed lines in Figure 6).

In addition, peptide bond-associated features in both IR and NMR spectroscopies, i.e., hypsochromic shifts of amide I bands and slight downfield shifts of Glu CO and Cys CO ^{13}C signals in the presence of U(VI), respectively, disclose changing conformation of the GSSG ligand (backbone) upon complexation of U(VI).

With regard to U(VI) and GSH speciation (Figures S1 and S2, SI), the two binary complexes forming in acid solution are $UO_2(H_2GSH)^{2+}$ and $UO_2(HGSH)^{+}$, predominating below and above pD ≈ 2.5, respectively, thereby reflecting the commencing deprotonation of GSH's Gly COOH. Accordingly, the solid lines in Figure S17, SI, mirror the growing contents of aqueous U(VI)–GSH complexes. At pD between 3 and 3.5, depending on the metal to ligand ratio, the curves show a break, and the $\Delta_U\delta_H$ values decline remarkably (dashed lines). In this pD range the speciation of both GSH and U(VI) changes significantly. On the one hand, U(VI) hydrolysis species per se reduce observable $\Delta_U\delta$ values owing to decreased Lewis acidity. On the other hand, GSH now predominates as a net monoanionic species, whereupon the concomitantly observed precipitation is not surprising. The yield of net neutral and, thus, hardly soluble complex species is more prevalent for GSH as compared to GSSG since the former possesses only half the number of ionizable functional groups. Considering both ligand and metal contents remaining dissolved (Figure S19, SI), GSH and U(VI) are unequally removed from solution, i.e., excessive in uranium, suggesting that the precipitates contain polynuclear species. Accordingly, the fraction of free GSH increases and the $\Delta_U\delta_H$ values decrease. Unlike GSSG, GSH cannot outcompete U(VI) hydrolysis and thus scarcely forms soluble ternary complexes.

Additionally, broadened NMR signals are a prominent feature, particularly for systems with significant U(VI) interaction, while the line width, $\Delta\nu_{1/2}$, denoting the width of the signal at half amplitude, is constantly small (about 0.7 Hz) in the blank spectra. However, the closer the probed nucleus to uranium's binding site, the larger is $\Delta\nu_{1/2}$. Rising [U(VI)] or pD reduces the competition between U(VI) and D^+ for COO^- and, correspondingly, slows down the exchange rate, the latter denoting the frequency of association and dissociation. For these processes take place on time scales whose inverse (in units of frequency) correspond to NMR spectral widths, the signals are affected in position and line width. Accordingly, the regime shifts from fast intermediate to slow intermediate exchange, with the respective rate becoming less than half the frequency difference of signals related to the exchanging sites. Taking up the measured maximal $\Delta_U\delta_H$ value of 140 Hz (pD 3.25 spectrum in Figure S15, SI) as the corresponding spectral distance between Gly α ^1H signals of U(VI)-bound and free GSH, the exchange rate is approximately 10^2 s^{-1}.

CONCLUSIONS

We investigated the coordination of U(VI) by the oligopeptides GSSG and GSH by means of complementary spectroscopic methods. Examination of complex formation and dynamics as well as binding fashion was examined from both the ligands' (NMR and IR) and the metal's perspective (TRLFS and IR). The results showed an excellent internal consistency between both different spectroscopic methods and speciation (changes) observed for the different (aqueous and solid) phases. For the first time the complex formation constant for the binary $UO_2(H_3GSSG)^+$ complex was determined.

The ligands' COO groups coordinate U(VI), whereas those of the Glu residues are more easily accessible, and those of the Gly residues are more capable. That means, even for low pD values U(VI) interacts with Glu COO, however, as of pD values in the order of

magnitude of its pK_a (pD ≈ 2.5), the Gly COO is the stronger binding site. Nonetheless, the Glu COO retains metal ion interaction. The Gly terminus thereby acts like a conventional carboxylic acid binding bidentately, whereas the Glu terminus (up to alkaline conditions) features a zwitterionic residue coordinating monodentately. On the one hand, by dint of their function *in vivo*, both GSH and GSSG are important ligands to be considered by themselves. On the other hand, for both constitute ambidentate ligands comprising the ability to bind in different coordination fashion, they are well-suited small model molecules resembling larger peptides or mimicking the functionalities on cell surfaces of, e.g., microorganisms. In this context, but also conceivable for many other applications beyond biota, GSH's free thiol group may be used for covalent attachment to suited surfaces rendering the carboxyl groups accessible for U(VI) sequestration or further derivatization.

In contrast to the intensively investigated GSH/GSSG–transition metal systems, the U(VI) containing system has three major peculiarities impacting complexation behavior: (i) strong hydrolysis of U(VI), (ii) linear dioxo structure of the uranyl ion imposing orbital requirements on coordination geometry, and (iii) exclusive O-donor ligation by the carboxylates in the first coordination sphere.

To either of the U(VI)–GSH and U(VI) –GSSG systems applies the observation of precipitation when net neutral complexes form. Especially when no further counter ions such as Cl^- or Na^+ are required for charge balancing the solubility is remarkably reduced resulting in high U(VI) removal from solution. The precipitates reflect the actual speciation of both the ligand and the metal, hence they contain binary complexes forming in acidic media, and ternary complexes obtained under slightly acidic through alkaline conditions, even in the presence of carbonate. The largest quantities of soluble U(VI)–GSSG/GSH complexes are detected between pD 3 and 4. Although as of pD 6 quite stable uranyl carbonate complexes emerge, GSSG can compete upon formation of polynuclear ternary complexes of increased solubility. Therefore, solubility of the formed complexes is the result of the interplay between speciation of both U(VI) and the ligands. Consequently, especially GSSG and, thus, other (oligo) peptides can promote U(VI) mobilization or immobilization, strongly contingent on the complexes' net charges.

The experimental approach used in this work allowed for the derivation of the complex formation constant $\log K^{\circ} = 5.24 \pm 0.08$ for the reaction $UO_2^{2+} + H_3GSSG^- \rightarrow UO_2(H_3GSSG)^+$ at infinite dilution. These extensions of the thermodynamic database for organic uranyl(VI) compounds now enables more reliable speciation calculation in the respective chemical systems.

By examining the interaction between U(VI) being released naturally or deliberately into the environment, and potential targets in living beings, GSH and GSSG are bridge-building between studies *in vitro* and *in vivo*. Hence, the presented results advance the knowledge in bio-ligand coordination to U(VI). The results may be transferred to other actinyl ions (Np, Pu), helping to understand both basic aqueous coordination chemistry of high-valent f-elements and detoxification mechanisms as well as to develop remediation procedures.

In light of high tolerances of some organisms for very acidic conditions and high radionuclide concentrations as in flooded uranium mines or nuclear waste tanks,[79-82] it would be very interesting to check whether the results obtained for GSH/GSSG (or related compounds) may provide a clue on the operating detoxification mechanisms in such extremophiles.

ASSOCIATED CONTENT

Supporting Information

Calculated aqueous speciation distribution diagrams for U(VI) under both ambient and N_2 atmosphere as well as for GSH and GSSG, stability constant determination via Stern-Volmer plot and refinement by PARAFAC, GSH–U(VI) ^{1}H, and GSSG–U(VI) ^{1}H and ^{13}C NMR spectra for varying either pD for given M/L, or [U(VI)] for given pD, as well as analyses of both metal and ligand contents remaining in solution. This material is available free of charge via the Internet at http://pubs.acs.org.

AUTHOR INFORMATION

Corresponding Author

* E-mail: j.kretzschmar@hzdr.de

Present Addresses

† Helmholtz-Zentrum Dresden-Rossendorf, Institute of Ion Beam Physics and Materials Research, Bautzner Landstr. 400, 01328 Dresden, Germany.

‡ Institute of Chemistry, University Potsdam, Karl-Liebknecht-Str. 24-25, Building 29, 14476 Potsdam OT Golm, Germany.

Author Contributions

The manuscript was written through contributions of all authors. All authors have given approval to the final version of the manuscript.

Notes

The authors declare no competing financial interests.

ACKNOWLEDGMENT

The German Federal Ministry for Economic Affairs and Energy (BMWi) is acknowledged for financial support (JK) under the contract no. 02 E 11415B. The authors are grateful to Harald Foerstendorf for discussions on IR spectra, Stephan Weiß for his valuable support in the lab, Karsten Heim for IR performance, as well as Carola Eckardt and Aline Chlupka for TOC and ICP-MS measurements.

ABBREVIATIONS

Cys, cysteinyl residue; Glu, glutamyl residue; Gly, glycyl residue; GSH, glutathione, γ-(L)-glutamyl-(L)-cysteinylglycine; GSSG, glutathione disulfide, oxidized glutathione; FT-IR, Fourier-transform infrared spectroscopy; NMR, nuclear magnetic resonance spectroscopy; PARAFAC, parallel factor analysis; ppb, parts per billion; ppm, parts per million; U(VI), hexavalent uranium; TRLFS time-resolved laser-induced fluorescence spectroscopy.

REFERENCES

1. Meister, A.; Anderson, M. E., Glutathione. *Annu. Rev. Biochem* **1983,** *52* (1), 711-760.
2. Pompella, A.; Visvikis, A.; Paolicchi, A.; De Tata, V.; Casini, A. F., The changing faces of glutathione, a cellular protagonist. *Biochem. Pharmacol.* **2003,** *66* (8), 1499-1503.
3. Sies, H., Glutathione and its role in cellular functions. *Free Radical Biol. Med.* **1999,** *27* (9–10), 916-921.
4. Dringen, R., Metabolism and functions of glutathione in brain. *Progress in Neurobiology* **2000,** *62* (6), 649-671.
5. Bodansky, D., *Nuclear Energy: Principles, Practices, and Prospects*. 2nd ed.; Springer: New York, 2005.
6. Forsberg, C. W., Effect of depleted-uranium dioxide particulate fill on spent-nuclear-fuel waste packages. *Nucl. Technol.* **2000,** *131* (3), 337-353.
7. Landa, E. R.; Gray, J. R., US Geological Survey research on the environmental fate of uranium mining and milling wastes. *Environ. Geol.* **1995,** *26* (1), 19-31.
8. Baumann, N.; Arnold, T.; Foerstendorf, H.; Read, D., Spectroscopic Verification of the Mineralogy of an Ultrathin Mineral Film on Depleted Uranium. *Environ. Sci. Technol.* **2008,** *42* (22), 8266-8269.
9. Baumann, N.; Arnold, T.; Geipel, G.; Trueman, E. R.; Black, S.; Read, D., Detection of U(VI) on the surface of altered depleted uranium

by time-resolved laser-induced fluorescence spectroscopy (TRLFS). *Sci. Total Environ.* **2006,** *366* (2), 905-909.

10. Kidd, P. M., Glutathione: systemic protectant against oxidative and free radical damage. *Altern. Med. Rev.* **1997,** *2* (3), 155–176.

11. Raha, A.; Tew, K. D., Glutathione S-Transferases. In *Drug Resistance*, Hait, W. N., Ed. Springer US: 1996; Vol. 87, pp 83-122.

12. Singh, B. K., Complexation Behaviour of Glutathione with Metal Ions. *Asian J. Chem.* **2005,** *17* (1), 1-32.

13. Ketterer, B.; Coles, B.; Meyer, D. J., The role of glutathione in detoxication. *Environ. Health Perspect.* **1983,** *49*, 59-69.

14. Viehweger, K.; Geipel, G.; Bernhard, G., Impact of uranium (U) on the cellular glutathione pool and resultant consequences for the redox status of U. *BioMetals* **2011,** *24* (6), 1197-1204.

15. Vanhoudt, N.; Vandenhove, H.; Smeets, K.; Remans, T.; Van Hees, M.; Wannijn, J.; Vangronsveld, J.; Cuypers, A., Effects of uranium and phosphate concentrations on oxidative stress related responses induced in Arabidopsis thaliana. *Plant Physiol. Biochem.* **2008,** *46* (11), 987-996.

16. Vandenhove, H.; Cuypers, A.; Van Hees, M.; Koppen, G.; Wannijn, J., Oxidative stress reactions induced in beans (Phaseolus vulgaris) following exposure to uranium. *Plant Physiol. Biochem.* **2006,** *44* (11–12), 795-805.

17. Cassier-Chauvat, C.; Chauvat, F., Responses to Oxidative and Heavy Metal Stresses in Cyanobacteria: Recent Advances. *Int. J. Mol. Sci.* **2014,** *16* (1), 871-886.

18. Gschneidner Jr., K. A.; Eyring, L.; Choppin, G. R.; Lander, G. H., *Handbook on the Physics and Chemistry of Rare Earths*. Elsevier B.V.: Amsterdam, 1994; Vol. 18: Lanthanides/Actinides: Chemistry.

19. Duffield, J. R.; Taylor, D. M., The biochemistry of the actinides. In *Handbook on the Physics and Chemistry of the Actinides*, Freeman, A. J.; Keller, C., Eds. Elsevier B.V.: Amsterdam, 1986; Vol. 4.

20. Popplewell, D. S.; Stradling, G. N.; Ham, G. J., The Chemical Form of Plutonium in Urine. *Rad. Res.* **1975,** *62*, 513-519.

21. Krężel, A.; Szczepanik, W.; Sokołowska, M.; Jeżowska-Bojczuk, M.; Bal, W., Correlations between Complexation Modes and Redox Activities of Ni(II)−GSH Complexes. *Chem. Res. Toxicol.* **2003,** *16* (7), 855-864.

22. Shoukry, M. M., Complex formation equilibria between mercury(II) complexes of pencillamine and glutathione and transition metal ions. *Transition Met. Chem.* **1990,** *15* (1), 1-4.

23. Mah, V.; Jalilehvand, F., Lead(II) Complex Formation with Glutathione. *Inorg. Chem.* **2012,** *51* (11), 6285-6298.

24. Leung, B. O.; Jalilehvand, F.; Mah, V.; Parvez, M.; Wu, Q., Silver(I) Complex Formation with Cysteine, Penicillamine, and Glutathione. *Inorg. Chem.* **2013,** *52* (8), 4593-4602.

25. Levina, A.; Lay, P. A., Solution Structures of Chromium(VI) Complexes with Glutathione and Model Thiols. *Inorg. Chem.* **2004,** *43* (1), 324-335.

26. Shtyrlin, V. G.; Zyavkina, Y. I.; Ilakin, V. S.; Garipov, R. R.; Zakharov, A. V., Structure, stability, and ligand exchange of copper(II) complexes with oxidized glutathione. *J. Inorg. Biochem.* **2005,** *99* (6), 1335-1346.

27. Aliaga, M. E.; López-Alarcón, C.; Bridi, R.; Speisky, H., Redox-implications associated with the formation of complexes between copper ions and reduced or oxidized glutathione. *J. Inorg. Biochem.* **2016,** *154*, 78-88.

28. Krężel, A.; Wójcik, J.; Maciejczyk, M.; Bal, W., Zn(II) Complexes of Glutathione Disulfide: Structural Basis of Elevated Stabilities. *Inorg. Chem.* **2011,** *50* (1), 72-85.

29. Bismondo, A.; Rizzo, L., Thermodynamics of the complex formation between uranyl(VI) and some polypeptides in aqueous solution. *Thermochim. Acta* **1992,** *196* (1), 131-136.

30. Frost, L.; Geipel, G.; Viehweger, K.; Bernhard, G., Interaction of uranium(VI) towards glutathione – an example to study different functional groups in one molecule. *Proc. Radiochim. Acta* **2011,** *1* (1), 357-362.

31. Obeid, M. H.; Oertel, J.; Solioz, M.; Fahmy, K., Mechanism of Attenuation of Uranyl Toxicity by Glutathione in *Lactococcus lactis*. *Appl. Environ. Microbiol.* **2016,** *82* (12), 3563.

32. Yue, Y.-C.; Li, M.-H.; Wang, H.-B.; Zhang, B.-L.; He, W., The toxicological mechanisms and detoxification of depleted uranium exposure. *Environ. Health Prev. Med.* **2018,** *23* (1), 18.

33. Kretzschmar, J.; Haubitz, T.; Hübner, R.; Weiss, S.; Husar, R.; Brendler, V.; Stumpf, T., Network-like arrangement of mixed-valence uranium oxide nanoparticles after glutathione-induced reduction of uranium(VI). *Chem. Commun.* **2018,** *54* (63), 8697-8700.

34. Kretzschmar, J.; Brendler, E.; Wagler, J.; Schmidt, A.-C., Kinetics and activation parameters of the reaction of organoarsenic(V) compounds with glutathione. *J. Hazard. Mater.* **2014,** *280*, 734-740.

35. Mirzahosseini, A.; Somlyay, M.; Noszál, B., The comprehensive acid–base characterization of glutathione. *Chem. Phys. Lett.* **2015,** *622*, 50-56.

36. Noszál, B.; Szakács, Z., Microscopic Protonation Equilibria of Oxidized Glutathione. *J. Phys. Chem. B* **2003,** *107* (21), 5074-5080.

37. Kresge, A., Solvent isotope effect in H2O–D2O mixtures. *Pure Appl. Chem* **1964,** *8*, 243-258.

38. Mikkelsen, K.; Nielsen, S. O., Acidity measurements with the glass electrode in H2O-D2O mixtures. *J. Phys. Chem.* **1960,** *64* (5), 632-637.

39. Harshman, R., Foundations of the PARAFAC procedure: Models and conditions for an ``explanatory'' multi-modal factor analysis. *UCLA Working Papers in Phonetics* **1970,** *16*, 1-84.

40. Carroll, J. D.; Chang, J.-J., Analysis of individual differences in multidimensional scaling via an n-way generalization of "Eckart-Young" decomposition. *Psychometrika* **1970,** *35* (3), 283-319.

41. Andersson, C. A.; Bro, R., The N-way Toolbox for MATLAB. *Chemom. Intell. Lab. Syst.* **2000,** *52* (1), 1-4.

42. Drobot, B.; Bauer, A.; Steudtner, R.; Tsushima, S.; Bok, F.; Patzschke, M.; Raff, J.; Brendler, V., Speciation Studies of Metals in Trace Concentrations: The Mononuclear Uranyl(VI) Hydroxo Complexes. *Anal. Chem.* **2016,** *88* (7), 3548-3555.

43. Drobot, B.; Steudtner, R.; Raff, J.; Geipel, G.; Brendler, V.; Tsushima, S., Combining luminescence spectroscopy, parallel factor analysis and quantum chemistry to reveal metal speciation – a case study of uranyl(VI) hydrolysis. *Chem. Sci.* **2015,** *6* (2), 964-972.

44. Schott, J.; Kretzschmar, J.; Tsushima, S.; Drobot, B.; Acker, M.; Barkleit, A.; Taut, S.; Brendler, V.; Stumpf, T., The interaction of Eu(III) with organoborates - a further approach to understand the complexation in the An/Ln(III)-borate system. *Dalton Trans.* **2015,** *44* (24), 11095-11108.

45. Alderighi, L.; Gans, P.; Ienco, A.; Peters, D.; Sabatini, A.; Vacca, A., Hyperquad simulation and speciation (HySS): a utility program for the investigation of equilibria involving soluble and partially soluble species. *Coord. Chem. Rev.* **1999,** *184*, 311-318.

46. Guillaumont, R.; Fanghänel, T.; Fuger, J.; Grenthe, I.; Neck, V.; Palmer, D. A.; Rand, M. H.; OECD/NEA, *Update on the Chemical Thermodynamics of Uranium, Neptunium, Plutonium, Americium and Technetium*. Elsevier: Amsterdam, 2003.

47. Günther, A.; Geipel, G.; Bernhard, G., Complex formation of uranium(VI) with the amino acids l-glycine and l-cysteine: A fluorescence emission and UV–Vis absorption study. *Polyhedron* **2007,** *26* (1), 59-65.

48. Davies, C. W., *Ion Association*. Butterworths: London, 1962.

49. Wang, Z.; Zachara, J. M.; Yantasee, W.; Gassman, P. L.; Liu, C.; Joly, A. G., Cryogenic Laser Induced Fluorescence Characterization of U(VI) in Hanford Vadose Zone Pore Waters. *Environ. Sci. Technol.* **2004,** *38* (21), 5591-5597.

50. Bader, M.; Rossberg, A.; Steudtner, R.; Drobot, B.; Großmann, K.; Schmidt, M.; Musat, N.; Stumpf, T.; Ikeda-Ohno, A.; Cherkouk, A., Impact of Haloarchaea on Speciation of Uranium—A Multispectroscopic Approach. *Environ. Sci. Technol.* **2018,** *52* (21), 12895-12904.

51. Zheng, Y.-Z.; Tong, M.-L.; Chen, X.-M., Synthesis, Structure and Photoluminescent Studies of Two Novel Layered Uranium Coordination Polymers Constructed from UO(OH) Polyhedra and Pyridinedicarboxylates. *Eur. J. Inorg. Chem.* **2005,** *2005* (20), 4109-4117.

52. Liao, Z.-L.; Li, G.-D.; Wei, X.; Yu, Y.; Chen, J.-S., Construction of Three-Dimensional Uranyl–Organic Frameworks with Benzenetricarboxylate Ligands. *Eur. J. Inorg. Chem.* **2010,** *2010* (24), 3780-3788.

53. Qian, W.; Krimm, S., Vibrational analysis of glutathione. *Biopolymers* **1994,** *34* (10), 1377-1394.

54. Podanyi, B.; Reid, R. S., NMR study of the conformations of free and lanthanide-complexed glutathione in aqueous solution. *J. Am. Chem. Soc.* **1988,** *110* (12), 3805-3810.

55. Clark, D. L.; Conradson, S. D.; Donohoe, R. J.; Keogh, D. W.; Morris, D. E.; Palmer, P. D.; Rogers, R. D.; Tait, C. D., Chemical Speciation of the Uranyl Ion under Highly Alkaline Conditions. Synthesis, Structures, and Oxo Ligand Exchange Dynamics. *Inorg. Chem.* **1999,** *38* (7), 1456-1466.

56. Quilès, F.; Burneau, A., Infrared and Raman spectra of uranyl(VI) oxo-hydroxo complexes in acid aqueous solutions: a chemometric study. *Vib. Spectrosc.* **2000,** *23* (2), 231-241.
57. Tsushima, S., On the "yl" bond weakening in uranyl(VI) coordination complexes. *Dalton Trans.* **2011,** *40* (25), 6732-6737.
58. Lu, G.; Haes, A. J.; Forbes, T. Z., Detection and identification of solids, surfaces, and solutions of uranium using vibrational spectroscopy. *Coord. Chem. Rev.* **2018,** *374*, 314-344.
59. Schlosser, F.; Krüger, S.; Rösch, N., A Density Functional Study of Uranyl Monocarboxylates. *Inorg. Chem.* **2006,** *45* (4), 1480-1490.
60. Ray, R. S.; Krüger, S.; Rösch, N., Uranyl monocarboxylates of aromatic acids: A density functional model study of uranyl humate complexation. *Dalton Trans.* **2009,** *0* (18), 3590-3598.
61. Quilès, F.; Burneau, A., Infrared and Raman spectroscopic study of uranyl complexes: hydroxide and acetate derivatives in aqueous solution. *Vibr. Spectrosc.* **1998,** *18* (1), 61-75.
62. Reitz, T.; Rossberg, A.; Barkleit, A.; Steudtner, R.; Selenska-Pobell, S.; Merroun, M. L., Spectroscopic study on uranyl carboxylate complexes formed at the surface layer of Sulfolobus acidocaldarius. *Dalton Trans.* **2015,** *44* (6), 2684-2692.
63. Barkleit, A.; Moll, H.; Bernhard, G., Complexation of uranium(VI) with peptidoglycan. *Dalton Trans.* **2009,** *0* (27), 5379-5385.
64. Deacon, G. B.; Phillips, R. J., Relationships between the carbon-oxygen stretching frequencies of carboxylato complexes and the type of carboxylate coordination. *Coord. Chem. Rev.* **1980,** *33* (3), 227-250.
65. Kakihana, M.; Nagumo, T.; Okamoto, M.; Kakihana, H., Coordination structures for uranyl carboxylate complexes in aqueous solution studied by IR and carbon-13 NMR spectra. *J. Phys. Chem.* **1987,** *91* (24), 6128-6136.
66. Lucks, C.; Rossberg, A.; Tsushima, S.; Foerstendorf, H.; Scheinost, A. C.; Bernhard, G., Aqueous Uranium(VI) Complexes with Acetic and Succinic Acid: Speciation and Structure Revisited. *Inorg. Chem.* **2012,** *51* (22), 12288-12300.
67. Benetollo, F.; Bombieri, G.; Herrero, P.; Rojas, R. M., Synthesis, thermogravimetry and X-ray analysis of uranyl benzoate and butyrate derivatives. *J. Alloys Compd.* **1995,** *225* (1), 400-405.
68. Serezhkin, V. N.; Grigor'ev, M. S.; Abdul'myanov, A. R.; Fedoseev, A. M.; Serezhkina, L. B., Synthesis and structure of U(VI), Np(VI), and Pu(VI) propionates. *Crystallogr. Rep.* **2015,** *60* (6), 844-852.
69. Savchenkov, A. V.; Vologzhanina, A. V.; Serezhkina, L. B.; Pushkin, D. V.; Serezhkin, V. N., The first uranyl complexes with valerate ions. *Acta Crystallogr., Sect. C: Cryst. Struct. Commun.* **2013,** *69* (7), 721-726.
70. Leciejewicz, J.; Alcock, N. W.; Kemp, T. J., Carboxylato complexes of the uranyl ion: Effects of ligand size and coordination geometry upon molecular and crystal structure. In *Coordination Chemistry*, Springer: Heidelberg, 1995; pp 43-84.
71. Feldman, I.; Koval, L., Reaction of the Uranyl Ion with Amino Acids. Bidentate Carboxylate Chelation. *Inorg. Chem.* **1963,** *2* (1), 145-150.
72. Sherry, A. D.; Pascual, E., Proton and carbon lanthanide-induced shifts in aqueous alanine. Evidence for structural changes along the lanthanide series. *J. Am. Chem. Soc.* **1977,** *99* (18), 5871-5876.
73. Szabó, Z.; Grenthe, I., Potentiometric and Multinuclear NMR Study of the Binary and Ternary Uranium(VI)−L−Fluoride Systems, Where L Is α-Hydroxycarboxylate or Glycine. *Inorg. Chem.* **2000,** *39* (22), 5036-5043.
74. Bismondo, A.; Rizzo, L.; Tomat, G.; Curto, D.; Di Bernardo, P.; Cassol, A., Thermodynamic properties of actinide complexes. Uranyl(VI)- and thorium(IV)-glycine systems. *Inorg. Chim. Acta* **1983,** *74*, 21-24.
75. Müller, K.; Brendler, V.; Foerstendorf, H., Aqueous Uranium(VI) Hydrolysis Species Characterized by Attenuated Total Reflection Fourier-Transform Infrared Spectroscopy. *Inorg. Chem.* **2008,** *47* (21), 10127-10134.
76. Frost, R. L.; Čejka, J., A Raman spectroscopic study of the uranyl carbonate rutherfordine. *J. Raman Spectrosc.* **2007,** *38* (11), 1488-1493.
77. Frost, R. L.; Čejka, J., A Raman spectroscopic study of the uranyl mineral rutherfordine—revisited. *J. Raman Spectrosc.* **2009,** *40* (9), 1096-1103.
78. Hoekstra, H. R.; Siegel, S., The uranium trioxide-water system. *J. Inorg. Nucl. Chem.* **1973,** *35* (3), 761-779.
79. Brown, A. R.; Boothman, C.; Pimblott, S. M.; Lloyd, J. R., The Impact of Gamma Radiation on Sediment Microbial Processes. *Appl. Environ. Microbiol.* **2015,** *81* (12), 4014.
80. Fredrickson, J. K.; Zachara, J. M.; Balkwill, D. L.; Kennedy, D.; Li, S.-m. W.; Kostandarithes, H. M.; Daly, M. J.; Romine, M. F.; Brockman, F. J., Geomicrobiology of high-level nuclear waste-contaminated vadose sediments at the hanford site, washington state. *Appl. Environ. Microbiol.* **2004,** *70* (7), 4230-4241.
81. Marques, C. R., Extremophilic Microfactories: Applications in Metal and Radionuclide Bioremediation. *Front. Microbiol.* **2018,** *9*, 1191-1191.
82. Seifert, J.; Erler, B.; Seibt, K.; Rohrbach, N.; Arnold, J.; Schlömann, M.; Kassahun, A.; Jenk, U., Characterization of the microbial diversity in the abandoned uranium mine Königstein. In *Uranium, Mining and Hydrogeology*, Merkel, B. J.; Hasche-Berger, A., Eds. Springer Berlin Heidelberg: Berlin, Heidelberg, 2008; pp 733-742.

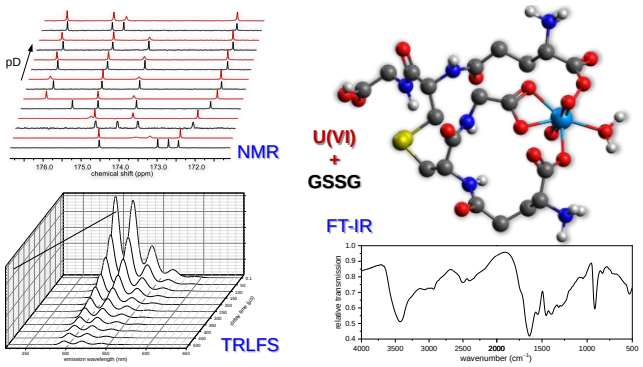

U(VI) interaction with glutathione and its dimer, glutathione disulfide, facilitates via the ligands' ambidentate carboxyl groups: the binding fashion depends on the terminus, i.e., monodentate coordination by the glutamyl and bidentate coordination by the glycyl residues, respectively. Complex solubility is the result of the interplay between speciation of both U(VI) and the peptides.